Chinese Chemical Letters 37 (2026) 110970

Contents lists available at ScienceDirect

Chinese Chemical Letters

journal homepage: www.elsevier.com/locate/cclet

CD44-targeting and ZIF-8 gated gold nanocage for programmed breast cancer therapy through Pt-induced immunogenic cell death

Xin Li[a], Fei Xiong[b], Xudong Cao[b], Wei Liu[b], Haobo Chen[b], Jiayu He[b], Weina Zhang[b], Longguang Tang[c,*], Wei Huang[b,d], Xikuang Yao[b,*]

[a] School of Pharmaceutical Science, Nanjing Tech University (NanjingTech), Nanjing 211816, China
[b] School of Flexible Electronics (Future Technologies) and Institute of Advanced Materials (IAM), Nanjing Tech University (NanjingTech), Nanjing 211816, China
[c] Gaozhou People's Hospital, Maoming 525200, China
[d] Frontiers Science Center for Flexible Electronics, Xi'an Institute of Flexible Electronics (IFE), Northwestern Polytechnical University (NPU), Xi'an 710072, China

ARTICLE INFO

Article history:
Received 5 December 2024
Revised 17 February 2025
Accepted 18 February 2025
Available online 19 February 2025

Keywords:
Programmed drug release
ZIF-8-gated
Gold nanocage
Immunogenic cell death
Cancer therapy

ABSTRACT

The field of nanomedicine has been revolutionized by the concept of immunogenic cell death (ICD)-enhanced cancer therapy, which holds immense promise for the efficient treatment of cancer. However, precise delivery of ICD inducer is severely hindered by complex biological barriers. How to design and build intelligent nanoplatform for adaptive and dynamic cancer therapy remains a big challenge. Herein, this article presents the design and preparation of CD44-targeting and ZIF-8 gated gold nanocage (Au@ZH) for programmed delivery of the 1,2-diaminocyclohexane-Pt(II) (DACHPt) as ICD inducer. After actively targeting the CD44 on the surface of 4T1 tumor cell, this Pt-Au@ZH can be effectively endocytosed by the 4T1 cell and release the DACHPt in tumor acidic environment, resulting in ICD effect and superior antitumor efficacy both *in vitro* and *in vivo* in the presence of mild 808 nm laser irradiation. By integration of internal and external stimuli intelligently, this programmed nanoplatform is poised to become a cornerstone in the pursuit of effective and targeted cancer therapy in the foreseeable future.

© 2025 Published by Elsevier B.V. on behalf of Chinese Chemical Society and Institute of Materia Medica, Chinese Academy of Medical Sciences.

Nowadays breast cancer has developed as a leading cause of the deaths of female patients around the word [1–3]. Especially, triple negative breast cancer as an extremely aggressive subtype can severely metastasize to the brain and elsewhere, which is quite difficult to cure [4–7]. Tremendous efforts have been devoted to exploit efficient method for diagnosis and treatment of breast cancer. Chemotherapy is still the main treatment for breast cancer in clinic. However, the efficacy is quite compromised and the patients usually suffer from serious side effects [8–10]. Notably, emerging cancer immunogenic cell death (ICD) has drawn great attention, ascribed to stimulated antitumor immunity [11–13]. By efficient delivery of ICD inducers, tumor cells can be eradicated and tumor associated antigens will be released, resulting in the maturation of dendritic cells and the recruitment of T cells [14]. Afterwards, efficient cancer treatment and the inhibition of cancer metastasis are expected to be achieved.

Notably, platinum (Pt) complexes including cisplatin and oxaliplatin have been widely utilized in clinic for efficient cancer treatment [15–19]. In general, these Pt-based anticancer drugs reveal appealing therapeutic efficacy through interaction with intranuclear gene nucleobases. What is more, recent studies demonstrate that oxaliplatin and its analogues can efficiently induce ICD effect by elevating intracellular oxidative stress [20–22]. However, serious side toxicities and frequent drug resistance have severely limited their application in clinic. Therefore, it is important to overcome biological barriers and delivery Pt-based anticancer drugs into tumor cells for precise ICD and cancer treatment. It is expected that these Pt complexes should be encapsulated well without leakage during the blood circulation time, while they should be efficiently released in tumor cells. Near infrared (NIR) light as a spatiotemporal control can precisely activate drug delivery nanosystem at the right place and at the right time, rendering a powerful strategy for Pt-based drug delivery [23–25]. A plenty of NIR-responsive nanomaterials have been constructed for cancer therapy. For instance, Xia *et al.* reported that gold nanocage with sub-100 nm had a favorable NIR absorption and hollow cavity, which showed appealing delivery of calcium ions (Ca^{2+}) and cell apoptosis [26]. For another,

* Corresponding authors.
E-mail addresses: tanglongguang@zju.edu.cn (L. Tang), iamxyao@njtech.edu.cn (X. Yao).

https://doi.org/10.1016/j.cclet.2025.110970
1001-8417/© 2025 Published by Elsevier B.V. on behalf of Chinese Chemical Society and Institute of Materia Medica, Chinese Academy of Medical Sciences.

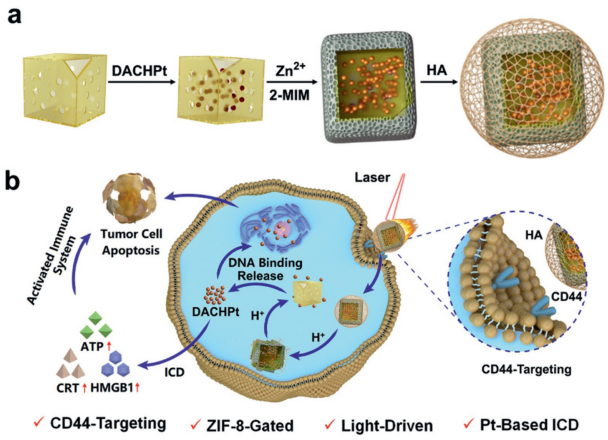


Fig. 1. Schematic illustration for the preparation of the Pt-Au@ZH (a) and the mechanism of Pt-enhanced ICD effect by the Pt-Au@ZH upon NIR laser (b).

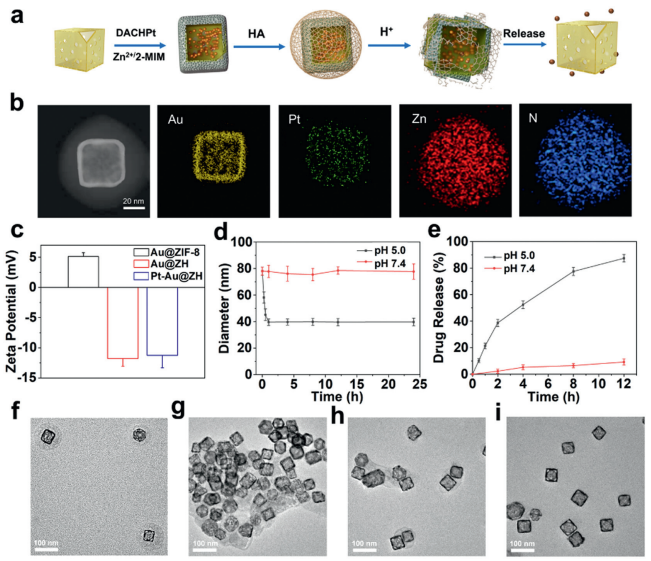


Fig. 2. Preparation and characterization of acid-sensitive Pt-Au@ZH. (a) Illustration for the preparation of Pt-Au@ZH and drug release behavior. (b) Element mapping images of Pt-Au@ZH. (c) The zeta potentials of Au@ZIF-8, Au@ZH and Pt-Au@ZH. (d) The stability of Pt-Au@ZH at different pH values. (e) Drug release behaviors of Pt-Au@ZH at pH 5.0 and pH 7.4. Typical TEM image of Pt-Au@ZH in PBS at pH 7.4 (f) and pH 5.0 for 15 min (g), 30 min (h) and 60 min (i). Scale bar: 100 nm. Data are presented as mean values ± SD ($n = 3$).

NIR-responsive gold nanovesicles could be fabricated by polymer-induced self-assembly of gold nanoparticles (NPs), which could load hydrophilic drugs in their cavities during the self-assembly [27]. Besides, tumor microenvironment (TME) including pH can be taken into account in the design of intelligent carriers. Due to high biocompatibility, easy modification and adjustable pore size, metal organic frameworks (MOFs) that are facilely prepared by interaction between metal ions and organic ligands have shown great potential for biomedical applications [28–31]. Especially, zeolitic imidazolate framework-8 (ZIF-8) can be mildly prepared and dissociated at a tumor acidic condition. Recent studies indicated that the stability and drug release behaviors of nanosystems could be greatly improved by ZIF-8 modification [32–34]. By integration of external stimulus and TME-sensitive function, programmed drug release is expected to be achieved as well as enhanced ICD efficacy and unfavored drug leakage can be avoided.

In this article, by integration of active tumor-targeting and NIR light-driven property, uniform CD44-targeted and ZIF-8 gated gold nanocage (Au@ZH) is designed and prepared for programmed delivery of 1,2-diaminocyclohexane-Pt(II) (DACHPt) (Fig. 1). DACHPt as parent drug of oxaliplatin has great potential for induction of ICD inside tumor cells. This Au@ZH is prepared by ZIF-8 coating on the surface of gold nanocage and subsequent hyaluronic acid (HA) modification. During the preparation, DACHPt can be encapsulated in the cavity of gold nanocage, affording DACHPt-loaded Au@ZH (Pt-Au@ZH). Due to overexpressed CD44 receptor on the surface of 4T1 cells, this Pt-Au@ZH is expected to efficiently target the tumor region [35–37]. Afterwards, this Pt-Au@ZH can be instantly endocytosed by 4T1 cells in the assistance of mild NIR light. Upon intracellular acidic environment, this Pt-Au@ZH can gradually get rid of the ZIF-8 layer and release DACHPt, resulting in superior antitumor efficacy and ICD effect. Prospectively, it is believed that this Pt-Au@ZH will pave a new way for the design and fabrication of precision nanomedicine in the future.

As shown in Fig. 2a, this Pt-Au@ZH was facilely prepared by encapsulation of DACHPt and sequential modification of pH-labile ZIF-8 and tumor-targeting HA. Firstly, Au nanocages with hollow structures were prepared by galvanic replacement reaction between Ag cubes and $HAuCl_4$ according to the protocol by Xia and coworkers (Fig. S1 in Supporting information) [38]. TEM images showed that uniform Ag nanocubes and as-obtained Au nanocages were prepared. After statistical analysis, it was concluded that those hollow gold cages had a length about 40.0 ± 3.0 nm and a thickness about 2.0 ± 0.6 nm, which were quite suitable for physical encapsulation of DACHPt in their cavities. Afterwards, ZIF-8 was coated on the surface of Au nanocages to prepare Au@ZIF-8. As shown in Fig. S2 (Supporting information), by adjusting the growing time, the thickness of ZIF-8 was precisely controlled to be 15 nm at 1 h, which was expected to protect encapsulated DACHPt from leakage. After ZIF-8 coating, HA was facilely modified on the surface for active tumor-targeting. As shown in Fig. S3 (Supporting information), the characteristic Fourier transform infrared spectroscopy (FT-IR) absorption peaks of HA at 3300 cm^{-1} (-OH) and 1675 cm^{-1} (C=O) were clearly observed in the Au@ZH and Pt-Au@ZH. More, the high-angle annular dark field scanning TEM and elemental mapping of Pt-Au@ZH determined that the ZIF-8 layer uniformly distributed on the surface of Au nanocage and the DACHPt was finely encapsulated in the core (Fig. 2b, Fig. S4 in Supporting information). The obtained Pt-Au@ZH had an average size of 78 nm with a dispersity index of 0.135 (Fig. S5 in Supporting information). Further, X-ray diffraction (XRD) analyses indicated that the pattern of the Au cage@ZIF-8 was consistent with the standard data of Au (JCPDS 04–0784) and calculated ZIF-8 (Fig. S6 in Supporting information). All these above results indicated that the Pt-Au@ZH was well prepared with appealing morphology and size.

Afterwards, the DACHPt loading content of Pt-Au@ZH was determined to be about 10.2 % by inductively coupled plasma-atomic emission spectrometry (ICP-AES). Ultraviolet–visible (UV–vis) absorption spectra revealed that the Pt-Au@ZH had a characteristic absorption peak around 750 nm, which was slightly red-shifted after ZIF-8 coating (Fig. S7 in Supporting information). What is more, the zeta potential of Pt-Au@ZH was turned to be negative −11.8 mV from positive 5.1 mV of that of Au@ZIF-8, indicating the successful modification of HA on the surface of Pt-Au@ZH (Fig. 2c). Further, the stability of the Pt-Au@ZH was investigated by DLS. As shown in Fig. 2d and Fig. S8 (Supporting information), the Pt-Au@ZH was quite stable in neutral environment with negligible size variation, while the hydrodynamic size decreased gradually upon an acid medium at pH 5.0, which was ascribed to the dissociation of ZIF-8 coating. This tumor acid-responsive property could greatly facilitate the DACHPt release in the intracellular environment. To quantitatively study the drug release property, the Pt-Au@ZH was dispersed in phosphate buffered saline (PBS) with various pHs. As

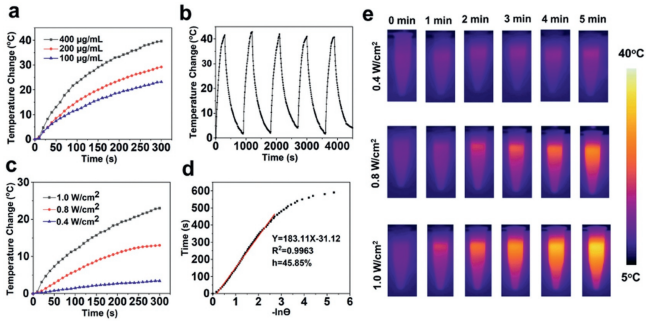


Fig. 3. (a) The heating curves of the Pt-Au@ZH at different concentrations with 1.0 W/cm^2 power density. (b) The photothermal cycle curves (400 μg/mL, 1.0 W/cm^2). (c) The heating curves of the Pt-Au@ZH at different power densities (100 μg/mL). (d) The time data *vs.* −lnθ of the Pt-Au@ZH obtained from the cooling period. (e) Typical images of 100 μg/mL Pt-Au@ZH irradiated by 808 nm laser with different power densities.

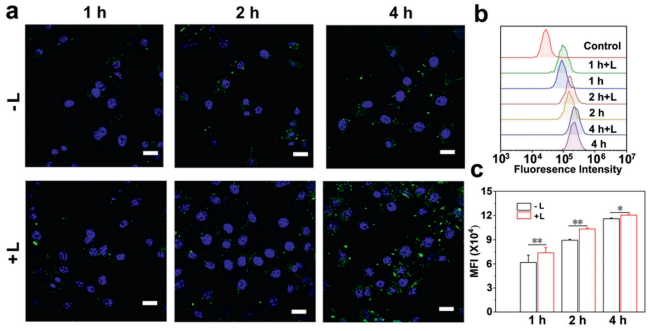


Fig. 4. (a) Typical CLSM images of 4T1 cells after treated with FITC-labeled Au@ZH for 1, 2 and 4 h in the absense or presence of 808 nm laser irradiation (0.4 W/cm^2, 5 min). L means laser irradiation.. Scale bar: 20 μm. (b) Quantitative analyses of 4T1 cell uptake efficiencies of the Au@ZH by flow cytometry. (c) MFI of 4T1 cells treated with FITC-labeled Au@ZH for different times in the presence or absence of 808 nm laser irradiation (0.4 W/cm^2, 5 min). Data are presented as mean values ± SD ($n = 3$). $^*P < 0.05$, $^{**}P < 0.01$.

demonstrated in Fig. 2e, <10% of loaded DACHPt was detected at pH 7.4 after incubation for 12 h, while >80% of DACHPt was released at pH 5.0 after incubation for 12 h, demonstrating attractive drug release behaviors of Pt-Au@ZH. Then, the morphology changes of the Pt-Au@ZH were monitored by TEM. Compared to intact ZIF-8 coating at the beginning, the ZIF-8 layer was completely damaged within 60 min at pH 5.0, which contributed to the prevention of DACHPt leakage at pH 7.4 and the controlled drug release of Pt-Au@ZH at acidic pH (Figs. 2f–i).

Next, to optimize the condition for mPTT-enhanced ICD effect *in vitro* and *in vivo*, the photo-thermal property of the Pt-Au@ZH in the presence of NIR 808 nm laser irradiation was carefully investigated. As shown in Fig. 3a, the temperature of the Pt-Au@ZH solution dramatically increased upon 808 nm laser irradiation. The temperature of the solution (400 μg/mL) was increased by >40 °C in the presence of 1.0 W/cm^2 808 nm laser for 5 min. Attractively, the Pt-Au@ZH possessed high stability with similar temperature increase during five heating-cooling cycles (Fig. 3b). To determine the mPTT condition, the photo-thermal property of the Pt-Au@ZH at different concentrations was also studied. As shown in Fig. 3c, the temperature of the solution could be increased below 5 °C at 100 μg and 0.4 W/cm^2 808 nm laser irradiation, which could be used for mPTT in the following experiments. The photothermal conversion was further calculated to be about 45.85% at this mild laser irradiation (Fig. 3d). Also, the images of the solution upon this laser irradiation visually revealed the heating process and temperature increase (Fig. 3e).

Considering the appealing photo-thermal property of the Pt-Au@ZH, the cell uptake behaviors of this nanoplatform was investigated accordingly. As shown in Fig. 4a, the fluorescein isothiocyanate (FITC) fluorescence intensity in 4T1 cells was gradually enhanced with increased incubation time, which visually indicated the Au@ZH was efficiently and continuously endocytosed by 4T1 cells. What is more, a bit more FITC-labeled Au@ZH nanoplatforms were observed in the cell cytoplasm in the presence of 808 nm laser irradiation, demonstrating that mild heat energy could efficiently facilitate and enhance the cell endocytosis of the Au@ZH. Furthermore, to quantitatively determine the cell uptake efficiency, 4T1 cells were characterized by flow cytometry after treated with FITC-labeled Au@ZH in the presence or absence of laser irradiation (808 nm laser, 0.4 W/cm^2, 5 min). As shown in Fig. 4b, the FITC fluorescence intensity of 4T1 cells in the presence of 808 nm laser irradiation was much higher than that in the absence of laser irradiation. The mean fluorescence intensity (MFI) of 4T1 cells in the presence of laser irradiation was 1.19, 1.16 and 1.04-fold of that in the absence of laser irradiation (Fig. 4c). These above results demonstrated that cell endocytosis barrier could be efficiently alle-

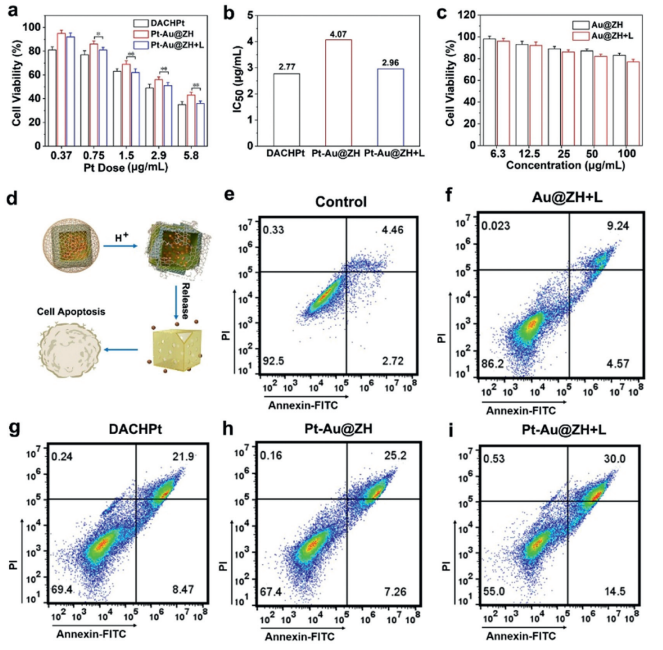


Fig. 5. *In vitro* antitumor efficacy of the Pt-Au@ZH. (a) The 4T1 cell viability after treated with different DACHPt concentrations as DACHPt, Pt-Au@ZH and Pt-Au@ZH in the presence or absence of laser irradiation (808 nm laser, 0.4 W/cm^2, 5 min). (b) IC_{50} values of DACHPt, Pt-Au@ZH and Pt-Au@ZH. (c) The biocompatibility of the Au@ZH in the presence or absence of laser irradiation. (d) Illustration for the mechanism of DACHPt release and subsequent cell apoptosis. The 4T1 cell apoptosis in the control group (e), the Au@ZH+L group (f), free DACHPt group (g), the Pt-Au@ZH group (h) and the Pt-Au@ZH+L group (i) (Pt dose: 6 μg/mL). Data are presented as mean values ± SD ($n = 6$). $^*P < 0.05$, $^{**}P < 0.01$.

viated by mild heat energy generated *via* NIR light, and the DACHPt was expected to be precisely delivered and exhibit therapeutic effect.

Afterwards, the therapeutic efficacy of the Pt-Au@ZH was investigated accordingly. As indicated in Fig. 5a, the 4T1 cell viability gradually decreased with increased DACHPt concentration. Due to acidic intracellular environment, the Pt-Au@ZH was able to release encapsulated DACHPt after endocytosis, and exhibited comparable antitumor efficacy to free DACHPt. What is more, the Pt-Au@ZH could eradicate 4T1 cells more efficiently upon mild laser irradiation, which was mainly ascribed to enhanced cell uptake of the Pt-Au@ZH and subsequent more DACHPt in the cytoplasm. The half maximal inhibitory concentration (IC_{50}) values of free DACHPt,

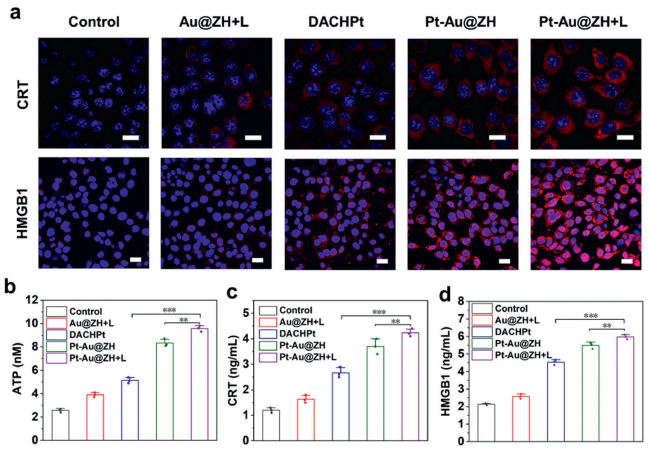


Fig. 6. *In vitro* ICD effect of the Pt-Au@ZH. (a) Typical CLSM images of CRT exposure on the surface 4T1 cells and HMGB1 release after treated with various formations. Scale bar: 20 μm. Quantitative analyses of the release of ATP (b), CRT (c) and HMGB1 (d) from 4T1 cells treated with various formations. Data are presented as mean values ± SD ($n = 3$). $^{**}P < 0.01$, $^{***}P < 0.001$.

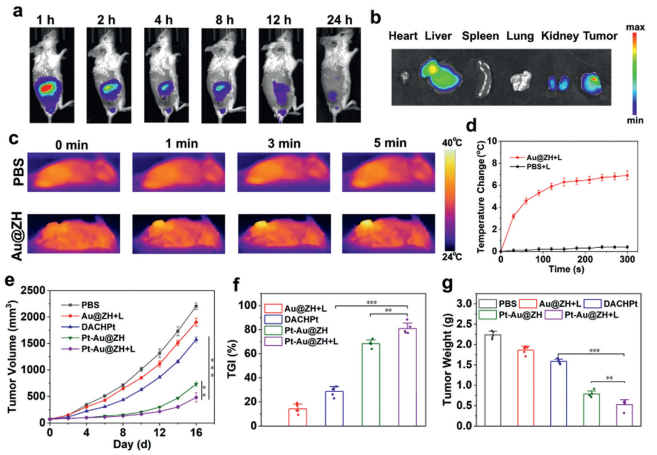


Fig. 7. (a) NIR Fluorescence (NIRF) images of 4T1 tumor bearing mice at different time points after tail vein injection of NIR-797 labeled Au@ZH. (b) fluorescence image of major organs and tumor after 24 h. (c) The photothermal images of 4T1 tumor bearing mice at different time points during the exposure of 808 nm NIR laser (0.4 W/cm^2, 5 min). (d) Temperature change curves after the tail vein injection of different formations in the presence of 808 nm NIR laser irradiation (0.4 W/cm^2, 5 min). (e) The tumor volume curves of 4T1 tumor-bearing mice during various treatments. (f) The TGI rate of different groups on day 16. (g) The tumor weights of 4T1 tumor-bearing mice after various treatments on day 16. Data are presented as mean values ± SD ($n = 5$). $^{**}P < 0.01$, $^{***}P < 0.001$.

Pt-Au@ZH and Pt-Au@ZH+L were 2.77, 4.07 and 2.96 μg/mL, respectively (Fig. 5b). Further, to evaluate the biocompatibility of the Au@ZH nanoplatform, 4T1 cells were incubated with the nanoplatform at various concentrations as high as 100 mg/mL in the presence or absence of laser irradiation. As shown in Fig. 5c, even the concentration of the Au@ZH reached as high as 100 mg/mL, the 4T1 cell viability was still above 80 %, illustrating high biocompatibility of the Au@ZH. Also, the Au@ZH and Pt-Au@ZH had very limited toxicity against normal NIH3T3 cells (Fig. S9 in Supporting information). And the Pt-Au@ZH had negligible influence on the red blood cells with no hemolysis occurred (Fig. S10 in Supporting information). More, the apoptosis of 4T1 cells receiving different treatments was analyzed (Fig. 5d). It was verified that the apoptotic ratio of 4T1 cells treated with Pt-Au@ZH+L were the highest as 30.0 % among all the groups, which was consistent with the MTT results (Figs. 5e–i).

Furthermore, to investigate the ICD effect of the Pt-Au@ZH *in vitro*, tumor associated antigens including adenosine triphosphate (ATP), calreticulin (CRT) and high mobility group box 1 (HMGB1) during various treatments were analyzed by confocal laser scanning microscope (CLSM) and enzyme-linked immunosorbent assay (ELISA) assays (Fig. 6). As revealed in Fig. 6a, the CRT red fluorescence on the surface of 4T1 cells and HMGB1 release were clearly observed after 4T1 cells treated with various formations. Notably, the 4T1 cells treated with the Pt-Au@ZH+L had the highest CRT and HMGB1 fluorescence intensity, demonstrating that the Pt-Au@ZH highly induced ICD effect of 4T1 cells in the presence of mild laser irradiation by greatly exposing CRT on their surface. Also, ELISA assays quantitatively indicated that the 4T1 cells treated with the Pt-Au@ZH+L had the highest amount excretion of ATP, CRT and HMGB1 (Figs. 6b–d). To be specific, the excretion of ATP from 4T1 cells treated with the Pt-Au@ZH+L was 1.87 and 1.15-fold of that treated with free DACHPt and the Pt-Au@ZH respectively (Fig. 6b). Accordingly, the excretion of CRT from 4T1 cells treated with the Pt-Au@ZH+L was 1.58 and 1.14-fold of that treated with free DACHPt and the Pt-Au@ZH respectively (Fig. 6c). And the excretion of HMGB1 from 4T1 cells treated with the Pt-Au@ZH+L was 1.32 and 1.09-fold of that treated free DACHPt and the Pt-Au@ZH respectively (Fig. 6d). All these above results revealed that the Pt-Au@ZH exhibited superior antitumor efficacy and induced distinct ICD effect *in vitro* in the presence of the mild 808 nm laser irradiation.

Considering the attractive antitumor efficacy *in vitro*, the *in vivo* biological behaviors of the Pt-Au@ZH were investigated by establishment of 4T1 tumor model. All involved animal experiments were conducted in accordance with the ethical regulations for animal experimentation and were approved by the Animal Experiment Institution of China Pharmaceutical University (CPU). Firstly, the biodistribution of the Au@ZH nanoplatform was visualized by *in vivo* fluorescence imaging after i.v. administration of the NIR dye (NIR797)-labeled nanoplatform. As shown in Fig. 7a, the Au@ZH was quickly captured by the liver at the beginning and gradually accumulated in tumor at 4 h. As the time went by, the fluorescence intensity in tumor increased greatly especially after 12 h i.v. injection. After 24 h, the tumor-bearing mice were dissected, and major organs and tumors were further imaged (Fig. 7b). It was observed that distinct NIR fluorescence was detected in tumor besides liver, indicating that the Au@ZH efficiently targeted and remained in tumor for at least 24 h. What is more, to optimize the laser irradiation intensity and time, the tumor-bearing mice were imaged during laser irradiation (Fig. 7c). Both the PBS group and the Au@ZH group were irradiated by 0.4 W/cm^2 808 nm laser for 5 min after i.v. injection for 12 h. Compared to the PBS group, the mice treated with the Au@ZH had an average temperature elevation about 6.9 °C in tumor, in which the *in situ* real temperature in tumor was below 40 °C (Fig. 7d). Therefore, the power density and irradiation time of 808 nm laser were set to be 0.4 W/cm^2 and 5 min in the following *in vivo* experiment.

Further, the *in vivo* antitumor efficacy of the Pt-Au@ZH was carefully evaluated in 4T1 tumor model. The 4T1 tumor-bearing mice were divided into five groups after the tumor volumes reached 75 mm^3. After i.v. administrated with various formations, the laser irradiation groups were treated with 0.4 W/cm^2 808 nm laser for 5 min. As illustrated in Fig. 7e, the tumor growth in the Pt-Au@ZH group and Pt-Au@ZH+L group was greatly inhibited when compared to that in the other groups, which was ascribed to active CD44-targeting on the surface of 4T1 cells and controlled DACHPt release in the intracellular environment. Especially, the Pt-Au@ZH+L treatment inhibited the tumor growth to the highest level among all the groups. The tumor growth inhibition (TGI) ratios of the Au@ZH+L, free DACHPt, Pt-Au@ZH and Pt-

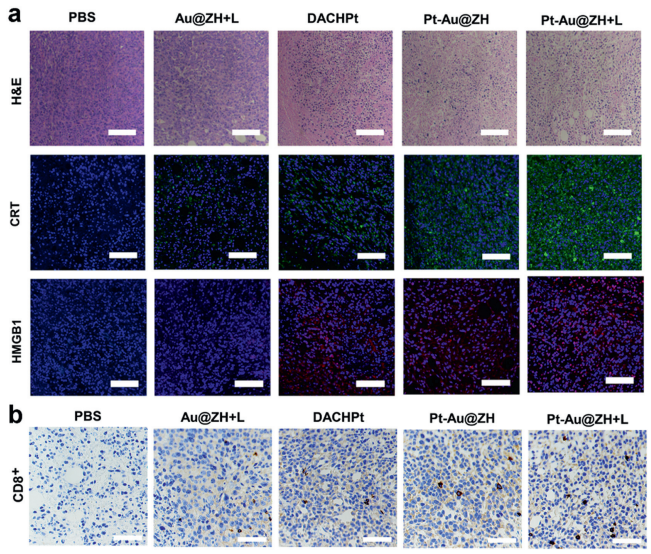


Fig. 8. (a) Representative images of H&E, CRT and HMGB1 expression of tumor tissues from 4T1 tumor-bearing mice treated with various formations, scale bar: 100 μm. (b) Representative images of $CD8^+$ T cells expression of tumor tissues from 4T1 tumor-bearing mice treated with various formations. Scale bar: 50 μm.

Au@ZH+L were calculated to be 12.8 %, 32.7 %, 68.5 % and 88.4 % respectively (Fig. 7f). During the treatments, the body weights of the mice were also monitored every other day. As shown in Fig. S11 (Supporting information), the Pt-Au@ZH had negligible influence on the living conditions of the tumor-bearing mice in the presence or absence of laser irradiation, which indicated minor side effects of the Pt-Au@ZH treatment. After day 16, all the living mice were dissected and the tumor weights in all the groups were measured accordingly. Notably, the tumors from the mice treated with the Pt-Au@ZH+L had the lightest weight, indicating that the Pt-Au@ZH extremely inhibited the tumor growth in the presence of mild laser irradiation (Fig. 7g). More, all the tumors were imaged, in which those from the mice treated with the Pt-Au@ZH+L had the smallest size among all the groups (Fig. S12 in Supporting information). All these above results revealed that this Pt-Au@ZH had the most powerful property in antitumor efficacy by combination of active CD44-targeting, programmed DACHPt release and mild NIR laser irradiation.

Nevertheless, after these above antitumor experiments, the dissected tumor tissues were further characterized by hematoxylin and eosin (H&E) and immunofluorescence. As shown in Fig. 8a, tumor tissues from the mice treated with the Pt-Au@ZH and Pt-Au@ZH+L exhibited severe nucleus shrinkage and tissue dissociation compared to the other groups, which was consistent with the superior antitumor efficacy of the Pt-Au@ZH and Pt-Au@ZH+L. Moreover, to evaluate the *in vivo* ICD effect, the expression of CRT and HMGB1 in tumor regions was carefully studied by immunofluorescence. Tumor tissues from the mice treated with the Pt-Au@ZH+L had the strongest CRT and HMGB1 signals among all the groups, which demonstrated the Pt-Au@ZH greatly induced ICD effect in the presence of the mild NIR laser irradiation (808 nm, 0.4 W/cm^2, 5 min). Furthermore, to evaluate the $CD8^+$ T cell infiltration in tumor after the ICD, the tumor tissues were characterized by immunohistochemical staining. As indicated in Fig. 8b, the tumors from the mice treated with the Pt-Au@ZH+L had the highest expression of $CD8^+$ T cells, indicating effective T cells infiltration. Meanwhile, the normal organs of the mice treated with the Pt-Au@ZH+L were also investigated by H&E. Compared to the PBS group, there was no obvious damage to normal tissues after the treatment of the Pt-Au@ZH+L (Fig. S13 in Supporting information). These above results revealed that the Pt-Au@ZH greatly inhibited the tumor growth in the presence of mild laser irradiation by induction of superior ICD effect with high biocompatibility.

In a word, active tumor-targeting and ZIF-8 gated gold nanocage was successfully prepared with uniform morphology and size distribution. The ICD inducer (DACHPt) was finely encapsulated in the cavity of gold nanocage with drug loading content about 10.2 %. This Pt-Au@ZH was quite stable in neutral biological environment and efficiently prevented the DACHPt from immature leakage. Upon acidic environment, the Pt-Au@ZH would gradually dissociate by destruction of the acid-labile ZIF-8 layer and quickly release the DACHPt in a sustained manner. Both *in vitro* and *in vivo* results revealed that this Pt-Au@ZH nanoplatform greatly enhanced cell endocytosis, exhibited distinct ICD effect and superior antitumor efficacy in the presence of mild NIR laser irradiation (0.4 W/cm^2 for 5 min). Therefore, it may bring a great chance for future construction of smart nanoplatform for precision nanomedicine.

Declaration of competing interest

The authors declare that they have no known competing financial interests or personal relationships that could have appeared to influence the work reported in this paper.

CRediT authorship contribution statement

Xin Li: Writing – review & editing, Writing – original draft, Methodology, Investigation, Data curation. **Fei Xiong:** Writing – original draft, Methodology, Investigation, Data curation. **Xudong Cao:** Writing – original draft, Methodology, Investigation, Data curation. **Wei Liu:** Writing – original draft, Methodology, Investigation, Data curation. **Haobo Chen:** Methodology, Investigation, Data curation. **Jiayu He:** Methodology, Investigation, Data curation. **Weina Zhang:** Writing – review & editing, Formal analysis. **Longguang Tang:** Writing – review & editing, Supervision, Project administration, Funding acquisition. **Wei Huang:** Writing – review & editing, Supervision, Project administration, Funding acquisition. **Xikuang Yao:** Writing – review & editing, Writing – original draft, Supervision, Project administration, Funding acquisition, Conceptualization.

Acknowledgments

This work was financially supported by the Natural Science Foundation of Jiangsu Province (No. BK20200709), the Natural Science Foundation of China (Nos. 62288102, 32201127 and 82270113), the Natural Science Foundation of Guangdong Province (No. 2023A1515011386), the Natural Science Foundation of the Jiangsu Higher Education Institutes (No. 20KJB430031), the startup fund from Nanjing Tech University, and Disciplinary Fund of School of Pharmaceutical Sciences (2024).

Supplementary materials

Supplementary material associated with this article can be found, in the online version, at doi:10.1016/j.cclet.2025.110970.

References

[1] J. Qi, M. Li, L. Wang, et al., Lancet Public Health 8 (2023) e943–e955.
[2] P.J. Gawne, M. Ferreira, M. Papaluca, et al., Nat. Rev. Mater. 8 (2023) 783–798.
[3] M. Qin, H. Xia, W. Xu, et al., Adv. Drug Deliv. Rev. 203 (2023) 115137.
[4] M.A. Harris, P. Savas, B. Virassamy, et al., Nat. Rev. Cancer 24 (2024) 554–577.
[5] S. Zhou, H. Tian, J. Yan, et al., Chin. Chem. Lett. 35 (2024) 108312.
[6] J. Liu, D. He, T. Hao, et al., Chin. Chem. Lett. 35 (2024) 109296.
[7] J. Zuo, X. Gao, J. Xiao, et al., Chin. Chem. Lett. 34 (2023) 107827.
[8] L.N.M. Nguyen, Z.P. Lin, S. Sindhwani, et al., Nat. Mater. 22 (2023) 1261–1272.
[9] B. Ouyang, W. Poon, Y.N. Zhang, et al., Nat. Mater. 19 (2020) 1362–1371.

[10] Q. Zhou, J. Xiang, N. Qiu, et al., Chem. Rev. 123 (2023) 10920–10989.
[11] P. Meier, A.J. Legrand, D. Adam, et al., Nat. Rev. Cancer 24 (2024) 299–315.
[12] N. Gong, M.G. Alameh, R. El-Mayta, et al., Nat. Rev. Drug Discov. 23 (2024) 607–625.
[13] P. Joyce, C.J. Allen, M.J. Alonso, et al., Nat. Nanotechnol. 19 (2024) 1597–1611.
[14] X. Yao, C. Sun, F. Xiong, et al., ACS Appl. Mater. Interfaces 16 (2024) 19472–19479.
[15] W. Liu, X. Li, T. Wang, et al., Small 19 (2023) 2208241.
[16] Z. Li, J. Zou, X. Chen, Adv. Mater. 35 (2023) 2209529.
[17] X. Zeng, J. Sun, S. Li, et al., Nat. Commun. 11 (2020) 567.
[18] J. Xiang, Y. Zhang, X. Liu, et al., Nano Lett. 22 (2022) 5615–5625.
[19] Q. Peña, A. Wang, O. Zaremba, et al., Chem. Soc. Rev. 51 (2022) 2544–2582.
[20] H. Lu, W. Tong, M. Jiang, et al., ACS Nano 18 (2024) 21156–21170.
[21] L. Zhang, K. Shang, X. Li, et al., Adv. Funct. Mater. 32 (2022) 2204589.
[22] X. Hu, R. Li, W. Wu, et al., J. Control. Release 348 (2022) 660–671.
[23] D. Wei, Y. Huang, B. Wang, et al., Angew. Chem. Int. Ed. 61 (2022) e202201486.
[24] J. Chen, L. Liu, S.M. Motevalli, et al., Adv. Funct. Mater. 28 (2018) 1707291.
[25] M. Zhou, J. Wang, J. Pan, et al., Nat. Commun. 14 (2023) 3593.
[26] Q. Chen, D. Huo, H. Cheng, et al., Adv. Healthc. Mater. 8 (2019) 1801113.
[27] R. Lv, Z. Qian, X. Zhao, et al., Nano Res. 16 (2023) 5685–5694.
[28] W. Yao, W. Liu, F. Su, et al., J. Am. Chem. Soc. 146 (2024) 18592–18605.
[29] X. Wan, H. Zhong, W. Pan, et al., Angew. Chem. Int. Ed. 58 (40) (2019) 14134–14139.
[30] A.K. Bindra, D. Wang, Y. Zhao, Adv. Mater. 35 (2023) 2300700.
[31] Z. Ma, Y. Zhang, X. Dai, et al., Adv. Mater. 33 (2021) 2104504.
[32] Y. Ma, Z. Su, L. Zhou, et al., Adv. Mater. 34 (2022) 2107560.
[33] Y. Tian, Z. Gao, N. Wang, et al., J. Am. Chem. Soc. 144 (2022) 18419–18428.
[34] K. Li, K. Xu, Y. He, et al., ACS Nano 17 (2023) 4667–4687.
[35] S.Z.F. Phua, G. Yang, W.Q. Lim, et al., ACS Nano 13 (2019) 4742–4751.
[36] Y. Lin, C. Li, A. Liu, et al., Biomater. Sci. 9 (2021) 1363–1373.
[37] X. Wang, R. Cheng, Z. Zhong, Acta Biomater. 125 (2021) 280–289.
[38] S.E. Skrabalak, L. Au, X. Li, Y. Xia, Nat. Protoc. 2 (2007) 2182–2190.